Draft version November 15, 2011
Preprint typeset using LaTeX style emulateapj v. 04/20/08

arXiv:1111.3199v1 [astro-ph.GA] 14 Nov 2011

$G0.253+0.016$: A MOLECULAR CLOUD PROGENITOR OF AN ARCHES-LIKE CLUSTER

Steven N. Longmore[1,2], Jill Rathborne[3], Nate Bastian[4], Joao Alves[5], Joana Ascenso[1], John Bally[7], Leonardo Testi[1], Andy Longmore[6], Cara Battersby[7], Eli Bressert[1,8], Cormac Purcell[9,10], Andrew Walsh[11], James Jackson[12], Jonathan Foster[12], Sergio Molinari[13], Stefan Meingast[5], A. Amorim[14], J. Lima[14], R. Marques[14], A. Moitinho[14], J. Pinhao[15], J. Rebordao[16], F. D. Santos[14]

[1]European Southern Observatory, Karl-Schwarzschild-Str. 2, 85748 Garching bei Munchen, Germany
[2]Harvard-Smithsonian Center for Astrophysics, 60 Garden Street, Cambridge, MA 02138, USA
[3]CSIRO Astronomy and Space Science, Epping, Sydney, Australia
[4]Excellence Cluster Universe, Boltzmannstr. 2, 85748 Garching, Germany
[5]University of Vienna, Türkenschanzstrasse 17, 1180 Vienna, Austria
[6]UK Astronomy Technology Centre, Edinburgh, UK
[7]Center for Astrophysics and Space Astronomy, University of Colorado, UCB 389, Boulder, CO 80309
[8]School of Physics, University of Exeter, Stocker Road, Exeter EX4 4QL, UK
[9]Department of Astronomy, University of Leeds, UK
[10]Sydney Institute for Astronomy (SiFA), School of Physics, The University of Sydney, NSW 2006, Australia
[11]Department of Astronomy, James Cook University, Townesville, Australia
[12]Institute for Astrophysical Research, Boston University, Boston, MA 02215, USA
[13]INAF, Rome, Italy
[14]SIM, Faculdade de Ciências da Universidade de Lisboa, Ed. C8. Campo Grande 1749-016 Lisbon, Portugal
[15]LIP-Coimbra, Department of Physics, University of Coimbra, 3004-516 Coimbra, Portugal
[16]CAAUL-FCUL, Ed. D. Est. Paco Lumiar 22, 1649-038 Lisbon, Portugal

Draft version November 15, 2011

ABSTRACT

Young massive clusters (YMCs) with stellar masses of $10^4-10^5\,\mathrm{M}_\odot$ and core stellar densities of 10^4-10^5 stars per cubic pc are thought to be the 'missing link' between open clusters and extreme extragalactic super star clusters and globular clusters. As such, studying the initial conditions of YMCs offers an opportunity to test cluster formation models across the full cluster mass range. $G0.253+0.016$ is an excellent candidate YMC progenitor. We make use of existing multi-wavelength data including recently available far-IR continuum (Herschel/Hi-GAL) and mm spectral line (HOPS and MALT90) data and present new, deep, multiple-filter, near-IR (VLT/NACO) observations to study $G0.253+0.016$. These data show $G0.253+0.016$ is a high mass ($1.3\times10^5\,\mathrm{M}_\odot$), low temperature ($\mathrm{T_{dust}}\sim$20 K), high volume and column density ($n\sim8\times10^4\,\mathrm{cm}^{-3}$; $\mathrm{N}_{H_2}\sim4\times10^{23}\,\mathrm{cm}^{-2}$) molecular clump which is close to virial equilibrium ($\mathrm{M_{dust}}\sim M_{\rm virial}$) so is likely to be gravitationally-bound. It is almost devoid of star formation and, thus, has exactly the properties expected for the initial conditions of a clump that may form an Arches-like massive cluster. We compare the properties of $G0.253+0.016$ to typical Galactic cluster-forming molecular clumps and find it is extreme, and possibly unique in the Galaxy. This uniqueness makes detailed studies of $G0.253+0.016$ extremely important for testing massive cluster formation models.

Subject headings: ISM: clouds — ISM: molecules — stars: formation — galaxies: star clusters

1. INTRODUCTION

One of the ground breaking discoveries of the Hubble Space Telescope was that massive stellar clusters, with properties that rival (or even exceed) those found in globular clusters in terms of mass and stellar density, are still forming in the universe today (Holtzman et al. 1992). These young massive clusters (YMCs) can be broadly defined as stellar clusters more massive than $10^4\,\mathrm{M}_\odot$ and with ages that are <100 Myr but that also exceed the current crossing time by a factor of a few, so are gravitationally-bound (see e.g. Ashman & Zepf 2001; Portegies Zwart et al. 2010) . The discovery of YMCs in the Galaxy has allowed a detailed study of their structural and stellar properties (e.g. Arches, Quintuplet, Westerlund 1 and 2, RSCG1, 2 and 3, GLIMPSE-CO1, NGC 3603: Figer et al. 1999; Clark et al. 2005; Ascenso et al. 2007; Figer et al. 2006; Davies et al. 2011; Beccari et al. 2010). Like their extragalactic counterparts, these Galactic YMCs have stellar masses of $10^4-10^5\,\mathrm{M}_\odot$ and core stellar densities of 10^4-10^5 stars per cubic pc. The stellar masses and densities are orders of magnitude larger than typical open clusters and comparable to those in globular clusters, super star clusters seen in merging/starburst galaxies and those inferred from observations of massive clusters forming at the epoch of peak star formation density ($z\sim2-3$) (Whitmore 2000; Johnson & Kobulnicky 2003; Swinbank et al. 2010; Danielson et al. 2011). As such, YMCs are potentially local-universe-analogs of these massive extragalactic and high-z stellar clusters. Within our own Galaxy, observations show a smooth continuum in the properties of young clusters, suggesting that YMCs merely represent the extreme end of the open cluster (OC) distribution function. Thus, understanding how YMCs form may provide a direct handle on i) globular and super star cluster formation, ii) cluster formation at the epoch of peak star

Electronic address: slongmor@eso.org

formation density ($z \sim 2-3$), iii) the most extreme conditions for star formation in the local universe, and iv) whether or not there are different formation modes across the cluster mass range.

Despite their importance, the formation process of YMCs is not well constrained observationally due to the lack of known potential gas clouds as progenitors. As a result it has not been possible to study the initial conditions of the molecular gas from which YMCs form (see e.g. Santangelo et al. 2009). Progress requires first finding and then deriving the properties of the most massive molecular gas clouds which are on the verge of forming YMCs. Such YMC progenitor clouds are expected to have a high mass ($\sim 10^5\,\mathrm{M}_\odot$) and small radii (a few pc) with high volume and column densities ($\gtrsim 10^4\,\mathrm{cm}^{-3}$; $\gtrsim 10^{23}\,\mathrm{cm}^{-2}$). Before the onset of star formation, the gas is also expected to be very cold ($\sim 10-20\,\mathrm{K}$). In order to resolve the internal structure of objects with radii $\sim$pc requires limiting the search to gas clouds within our own Galaxy.

Compared to the objects found in recent surveys of dense cluster-forming molecular clumps, one object, $\mathrm{G}0.253+0.016$, stands out as extreme (e.g. Sridharan et al. 2002; Hill et al. 2005; Beuther et al. 2002; Schuller et al. 2009; Bally et al. 2010; Aguirre et al. 2011; Molinari et al. 2010a; Rathborne et al. 2006; Simon et al. 2006a,b; Pillai et al. 2006; Peretto & Fuller 2009; Jackson et al. 2006; Rathborne et al. 2009; Longmore et al. 2007; Purcell et al. 2006, 2009; Walsh et al. 2008, 2011; Jackson et al. 2011). Identified as an infrared dark cloud (IRDC), it is clearly seen as a prominent extinction feature in mid-IR images (see Figure 1). Molinari et al. (2011) place $\mathrm{G}0.253+0.016$ in the "elliptical ring" feature orbiting the Galactic center, putting it $60-100\,\mathrm{pc}$ in front of the Galactic center, at a distance of $\sim$8.4 kpc (Reid et al. 2009). With a dust temperature of $\sim$20 K, volume density of $>10^4\,\mathrm{cm}^{-3}$, dust mass of $\sim 10^5\,\mathrm{M}_\odot$, and almost no signs of star-formation, $\mathrm{G}0.253+0.016$, has exactly the properties expected for the precursor to a massive, Arches-like cluster (Lis et al. 1994; Lis & Menten 1998; Lis et al. 2001; Bally et al. 2010).

Despite having the expected global properties for a YMC precursor, the dynamical state and fate of future star formation in $\mathrm{G}0.253+0.016$ remains uncertain. While the detection of a weak water maser suggests there may be a small number of low-mass stars forming (Lis et al. 1994), it is unclear whether the gas is globally bound and collapsing (and therefore going to form a massive cluster) or unbound and transient (Lis & Menten 1998). This ambiguity is complicated by the extreme environmental conditions within the Galactic center region (e.g. crowding, intense radiation fields, large magnetic fields, tidal shear). Given its importance as a potential precursor to a YMC, we make use of higher resolution and sensitivity data to study $\mathrm{G}0.253+0.016$ in detail and attempt to ascertain its dynamical state.

2. SURVEY DATA AND NEW OBSERVATIONS

2.1. *Survey data*

We make use of multi-wavelength archival data from the United Kingdom Infrared Digital Sky Survey (UKIDSS: Lawrence et al. 2007, data release 7), the Spitzer Galactic Legacy Infrared Mid-Plane Survey Extraordinaire (GLIMPSE: Benjamin et al. 2003), the Submillimetre Common-User Bolometer Array (SCUBA) on the James Clerk Maxwell Telescope (JCMT) (Di Francesco et al. 2008) and the methanol multi-beam survey (MMB: Caswell et al. 2010). We also make use of recently available data from the Herschel Infrared Galactic Plane Survey (HiGAL: Molinari et al. 2010b, 2011), the $\mathrm{H_2O}$ southern Galactic plane survey (HOPS: Walsh et al. 2008, 2011) and the Millimetre Astronomy Legacy Team 90 GHz Survey (MALT90: Jackson et al. 2011; Foster et al. 2011). Details of the surveys including observational parameters and references outlining the data acquisition/reduction procedures can be found in Table 1.

2.2. *VLT/NACO Observations*

Deep, near-IR data were obtained with the Nasmyth Adaptive Optics System Near-Infrared Imager and Spectrograph (NAOS-CONICA, or NACO) on the Very Large Telescope (VLT) on May 5th 2011. A field of view of $1' \times 1'$ centered on $17^h42^m58^s$, $-28^\circ 42' 23''$ (J2000) was imaged in J, H and K_s. Although offset from the nominal center of $\mathrm{G}0.253+0.016$, this position was chosen to be centered on a foreground star which was bright enough to use the Natural Guide Star adaptive optics system guiding with camera S54 and dichroic N20C80. After flatfielding and sky subtraction using IRAF[1] standard tools, the six dithered exposures of 10s each in each filter were shifted and combined into the final J, H and K_s images. The source extraction and PSF photometry were done with IRAF DAOPHOT using standard techniques and error cuts. We used Topcat[2] to match all the stars towards $\mathrm{G}0.253+0.016$ observed by VLT/NACO with the UKIDSS data (see § 3.1). Differences in filter wavelengths were corrected to first order using the principles described in Stead & Hoare (2009) and Appendix A of Schödel et al. (2010). Remaining uncertainties in color effects and from the statistical scatter mean the error in calibration is no more than ± 0.1 mag at each wavelength. The final NACO catalog contains 358, 1001 and 1830 sources, detected to the 5σ level up to 21.3, 20.5 and 19.8 mag in J, H and K_s, respectively. Despite the error cuts, up to 2% of the sources in the catalog in each filter are still spurious detections.

3. RESULTS

Figure 1 shows continuum images of $\mathrm{G}0.253+0.016$ at $3.6-8.0\mu$m, 70μm and 450μm. $\mathrm{G}0.253+0.016$ is elongated with an aspect ratio of approximately 3:1 and is seen as an extinction feature from 3.6 to 70μm with no obvious embedded emission sources. As such it must be both cold and dense and sit in front of the majority of the diffuse Galactic mid-IR background emission. At wavelengths $\geq 170\mu$m, bright emission is seen across $\mathrm{G}0.253+0.016$ (Molinari et al. 2011) with similar morphology to the 450μm emission shown in Figure 1. The lack of embedded emission sources at wavelengths up to 70μm combined with results from recent maser surveys which show no 6.7 GHz $\mathrm{CH_3OH}$ masers (Caswell et al.

---

[1] IRAF is distributed by the National Optical Astronomy Observatories, which are operated by the Association of Universities for Research in Astronomy, Inc., under cooperative agreement with the National Science Foundation.

[2] Taylor (2005): http://www.star.bris.ac.uk/~mbt/topcat/

TABLE 1
Summary of observational survey data used in this work

Survey/Archive	Telescope(s)	λ	continuum/line	θ	Reference(s)
UKIDSS	UKIRT	1.2, 1.6, 2.2 μm	continuum	$<1''$	Lawrence et al. (2007)
GLIMPSE	Spitzer	3.6, 4.5, 5.6, 8.0 μm	continuum	$2''$	Benjamin et al. (2003)
HiGAL	Herschel	70, 160, 250, 350, 500 μm	continuum	$5-36''$	Molinari et al. (2010b, 2011)
SCUBA Archive	JCMT	450, 850 μm	continuum	$8''$	(Di Francesco et al. 2008)
MALT90	Mopra	3 mm	line	$35''$	(Jackson et al. 2011; Foster et al. 2011)
HOPS	Mopra	12 mm	line	$2'$	(Walsh et al. 2008, 2011)
MMB	Parkes & ATCA	3 cm	line	$\sim1''$	(Caswell et al. 2010)

2010) or new 22 GHz H_2O maser detections (Walsh et al. 2011) strongly reinforces the paucity of active star formation within the cloud.

3.1. *Near-IR extinction*

From continuum observations alone it is not possible to determine whether the emission from G0.253 + 0.016 arises from a single physical entity or from multiple clouds along the same line of sight. Extinction measurements can be used to distinguish between these two scenarios. Additionally, given the confusion and the difficulty deriving kinematic distances towards the Galactic center, extinction measurements also offer an independent distance determination.

We used data from UKIDSS, specifically the Galactic Plane Survey (GPS: Lucas et al. 2008), and deep VLT/NACO observations (see § 2.2) to investigate the near-IR extinction towards G0.253 + 0.016. We downloaded the infrared sources in a $15'$ x $15'$ region centered on G0.253 + 0.016 from the UKIDSS data base, which allowed for a direct and coherent comparison of the cloud and off-cloud properties. The comparison of on- and off-source K_s *vs.* $(H - K_s)$ color-magnitude diagrams (CMDs) showed that there are far fewer very red stars in the direction of G0.253 + 0.016 than in any of the off-source diagrams, with a clear and maintained deficit in the number of red stars well established by $(H - K_s) = 1.7 \pm 0.2$ mag (see top panel of Figure 2)[3]. This is equally clearly seen when comparing the NACO data for G0.253 + 0.016 with similar field of view, albeit shallower, NACO observations toward the Galactic Centre by Schödel et al. (2010): Figure 2 shows the K_s *vs.* $(H - K_s)$ CMD, and the histogram of $(H - K_s)$ colors for that Galactic Centre field and for G0.253 + 0.016. Toward the Galactic center, the red giant branch bump feature is clearly seen extending to $(H - K_s) \sim 2.6$ mag, after which it is effected by completeness limits. However, despite being ∼2 mag deeper, the number of sources toward G0.253 + 0.016 drops rapidly above an $(H - K_s)$ of ∼1.7 mag, clearly showing that the extinction is produced by a sharp increase in dust density as expected from a dense cloud, as opposed to being produced by several low-density clouds along the line-of-sight which would be seen as a much more gradual decrease in the number of red stars.

We used the NACO data and Eq. 2 of Nishiyama et al. (2006) to estimate the distance to the cloud, using the red clump (RC) stars around $K_s \sim 15$ mag. We assume an absolute magnitude for the RC stars of $M_K = -1.54$ mag[4], a population correction $\Delta M_K = -0.07$, and the extinction law of Schödel et al. (2010) for the Galactic Centre ($A_\lambda \propto \lambda^{-2.21}$). The distance modulus is then given by $\mathrm{DM} = K - M_{K_s} + \Delta M_K$, where K is the observed, de-reddened K magnitude. We are looking for the distance to the near side of the cloud, so we used $(H - K_s) = 1.7$ mag to determine the extinction, since this is the color where we start to lose stars with respect to the Galactic Centre of Schodel et al. (2010) (see Figure 2, right-hand panel). Using the aforementioned extinction law, we derive $A_{K_s} = 2.13$ mag for an effective wavelength of 2.168μm, which, when applied to the observed magnitude of the RC stars ($K_{S,obs} = 15 \pm 0.3$ mag), yields a de-reddened $K_s = 12.87 \pm 0.3$ mag, or $K = 12.86 \pm 0.3$ considering the difference between K_s and K (Nishiyama et al. 2006). The distance modulus is then $\mathrm{DM} = 14.34 \pm 0.3$, translating into a distance of 7.4 ± 1.0 kpc and independently placing it just foreground of the Galactic Centre. The greatest source of uncertainty in this analysis is undoubtedly the extinction law, and we note that a difference of only 10% in the exponent of the extinction law in particular translates into an approximately 10% change in the derived distance.

In summary, based on the UKIDSS and NACO data we conclude that we have undoubtedly detected the extinction caused by G0.253 + 0.016, and that this is a single physical entity (as opposed to multiple clouds separated by large distances along the line of sight) with a distance consistent with being close in proximity to the Galactic Centre. Within the uncertainties, the IR-derived distance to G0.253 + 0.016 of 7.4 ± 1.0 kpc is consistent with the distance of 8.4 kpc that would be inferred if G0.253 + 0.016 is part of the "100 pc" ring orbiting the Galactic center, as proposed by Molinari et al. (2011). The distance to the "100 pc ring", in turn, is based on the distance to the Galactic center determined by Reid et al. (2009). As the formal uncertainty in the distance to the Galactic center is smaller than that from the IR-derived distance, we adopt a distance to G0.253+0.016 of 8.4 kpc for the remainder of the paper. The results of the paper remain valid if the nearer distance were adopted.

3.2. *Dust temperature, column density, radius and dust mass*

HiGAL data of the inner 2° × 2° of the Galactic center covering the Central Molecular Zone and G0.253 + 0.016 are presented by Molinari et al. (2011). Because continuum emission at these wavelengths is typically optically-thin and arises from the dust, we can use the Herschel data to derive the dust temperature and column density of G0.253 + 0.016.

---

[3] It should be noted that across the UKIDSS field examined there is also considerable variation in the foreground extinction, not surprising in a field so close to the Galactic Centre direction.

[4] We adopt the Schödel et al. (2010) value of $M_K = -1.54$ rather than that of $M_k = -1.59$ in Nishiyama et al. (2006) as we are directly comparing our data to the former.

The dust temperature and gas column density of G0.253 + 0.016 were estimated from a two-step pixel-to-pixel graybody fit to the Hi-GAL data. In the first coarse-angular-resolution step, graybody fits were calculated using the 170 - 500 μm data, scaled to the resolution of the 500 μm image ($\sim36''$). These results were used as inputs to the second, high-angular-resolution graybody fits to the 170 - 350 μm data, which were scaled to the resolution of the 350 μm image ($\sim25''$). Both steps used a fixed β of 1.75 and did not include the 70 μm point due to the high optical depth at this wavelength. The fitting method is similar to that described in Bernard et al. (2010) and Compiègne et al. (2011) but with the diffuse component of the emission removed (see Battersby et al. 2011, for full details on the methodology).

Figure 3 shows the derived dust temperature and column density maps. We find the dust temperature overall is low, increasing smoothly from $\sim$19 K at the center to $\sim$27 K at the edge. There are no obvious small pockets of heated dust from any embedded sources. The derived external temperature of G0.253 + 0.016 is significantly warmer ($\gtrsim$35 K).

The column density and dust temperature are anticorrelated as expected for an externally-heated, dense clump. The derived peak column density is $\sim3.3\times10^{23}$ cm^{-2} and decreases smoothly towards the edge. The cloud area was defined using a column density threshold of 3×10^{22} cm^{-2} which covers all the emission at T$\leq$ 27 K. Within this area the average column density is $\sim1\times10^{23}$ cm^{-2}. The emission is elongated with semi-major and semi-minor axes of $1.'9\times0.'7$, corresponding to a physical radius of 4.7$\times$1.7 pc for a distance of 8.4 kpc. Taking the geometric mean, we derive an effective radius of 2.8 pc for G0.253 + 0.016.

Given the strong dependence of dust emissivity with temperature and to account for the dust temperature variation across G0.253 + 0.016, we calculate the dust mass directly from the derived column density rather than from mm continuum emission which assumes a single dust temperature. The dust mass was calculated by multiplying the column density of each pixel by the pixel area, assuming a mean molecular weight of 2.8$\times$M$_{H-atom}$ (Kauffmann et al. 2008) and gas-to-dust ratio of 100:1 (Hildebrand 1983)[5], and summing over the pixels in the cloud area. The total mass is not particularly sensitive to the column density threshold, varying by <10% for threshold values of $1-5\times10^{22}$ cm^{-2}. We derive a dust mass for G0.253 + 0.016 of 1.3×10^5 M$_\odot$ and estimate the uncertainty to be of order 20%.

3.3. *Molecular line data: linewidth and virial mass*

To determine whether G0.253 + 0.016 is gravitationally-bound we compared the dust mass with the virial mass, M$_{\rm vir}$. M$_{\rm vir}$ is related to the measured radius, R, and linewidth, ΔV, through M$_{\rm vir}$ $\propto R\Delta V^2$, where the constant of proportionality depends on the geometry and gas density profile (MacLaren et al. 1988; Bertoldi & McKee 1992; Dunham et al. 2010). Clearly, small differences in linewidth can strongly affect the virial mass so it is important to ensure the measured linewidth reflects the underlying gas kinematics and has not been affected via other mechanisms (e.g. different excitation conditions, outflows, shocks, chemistry and optical-depth effects).

We used recently available data from the ongoing MALT90 molecular line survey (Jackson et al. 2011; Foster et al. 2011) to investigate the velocity structure of G0.253 + 0.016. Detailed analysis and modelling of the emission from the many detected molecular line transitions are underway and will be presented in a subsequent paper (Rathborne et al. in preparation). Here we focus on the global line properties with the aim of deriving the most reliable, representative linewidth for G0.253 + 0.016.

The brightest, optically-thick lines [e.g. HCO$^+$(1-0), HNC(1-0)] show the velocity structure towards this region is complicated. Emission is seen from several distinct velocity components over the spatial extent of G0.253 + 0.016 defined in § 3.2. The most prominent of these are: a component at $\sim$0 kms^{-1} seen at the north-east edge of the filament; a component at $\sim$35 kms^{-1} covering a similar emission area as the spatial extent of G0.253 + 0.016 defined above; and a component at $\sim$75 kms^{-1} seen towards the south west edge of the filament. Given the spatial extent of the 35 kms^{-1} component closely matches that of the dust emission, we take this component as the emission from G0.253 + 0.016, with the other components being from unrelated clouds along the line of sight.

The 35 kms^{-1} component shows evidence for shifts in the peak V$_{\rm lsr}$ with changes in spatial position (ie a velocity gradient). This means that taking a spectra from an individual spatial position would not accurately recover the integrated linewidth over the whole region, as the linewidth-broadening from the velocity gradient would not be taken into account. To overcome this requires extracting spectra which are integrated over the spatial extent of G0.253 + 0.016.

We selected bright, optically-thin emission as the most likely reliable tracer of the underlying gas kinematics. The top panel of Figure 4 shows Hanning-smoothed spectra from the H^{13}CO$^+$(1-0) and HN^{13}C(1-0) transitions integrated over the spatial extent of the cloud (as determined in § 3.2). The line profiles for both transitions are similar, giving confidence that they are robustly tracing the underlying gas kinematics. Both the V$_{\rm lsr}$ = 35 kms^{-1} component from G0.253 + 0.016 and the V$_{\rm lsr}$ = 0 kms^{-1} component are seen but the 75 kms^{-1} component is too faint in these optically-thin transitions to be detected. The bottom panel of Figure 4 shows the spatially-averaged HN^{13}C(1-0) emission with no Hanning smoothing. This emission was fit with a two-component Gaussian profile using the tasks within the CLASS[6] software package. To avoid biasing the fit results we did not constrain any of the parameters but rather left them all as free variables. From the resulting fits, which are overlayed on the spectra in the bottom panel of Figure 4, we derive the peak velocity and FWHM of the gas associated with $G0.253+0.016$ to be $V_{\rm lsr} = 36.1 \pm 0.4\,{\rm kms}^{-1}$ and $\Delta V = 15.1 \pm 1.0\,{\rm kms}^{-1}$, respectively. We adopt an upper limit linewidth of $16\,{\rm kms}^{-1}$ for $G0.253+0.016$ for the remainder of the paper.

---

[5] Due to the metallicity gradient in the disk (Balser et al. 2011), it is possible the gas-to-dust ratio in the CMZ may be lower than the canonical value of 100:1 commonly adopted in the literature. However, as individual metallicity measurements across the CMZ vary from 1 to $\sim$4 $\times$ Solar (Shields & Ferland 1994; Maeda et al. 2002; Najarro et al. 2009) and no independent measurements exist for G0.253 + 0.016, we opt for the standard gas-to-dust ratio of 100:1, while noting the dust-based mass may possibly be lower.

[6] CLASS is part of the GILDAS software environment: http://iram.fr/IRAMFR/GILDAS/

The derived virial mass can vary by an order of magnitude depending on the assumed geometry and density distribution. Assuming a spherical source with a density distribution $\propto r^{-2}$ gives a virial mass estimate of $9{\times}10^4\,{\rm M}_\odot$ (MacLaren et al. 1988, Eq 3). However, more realistically, for a centrally-condensed cloud elongated with axis ratio 3:1 and density $\propto r^{-1.8}$, the virial mass would be $4{\times}10^5\,{\rm M}_\odot$ (Bertoldi & McKee 1992; Dunham et al. 2010). Despite the assumptions and systematic uncertainties, the dust and virial mass estimates agree to within a factor of a few. Thus it is likely $G0.253+0.016$ is close to virial equilibrium.

4. DISCUSSION

The global properties of $G0.253+0.016$ derived in § 3 are summarized in Table 2. Based on these results, $G0.253+0.016$ is a strong candidate precursor of an Arches-like YMC. The only other two similar Galactic YMC-forming clouds that have been studied to date are Sgr B2 and W49A (e.g. Goldsmith et al. 1990; Alves & Homeier 2003). However, these are both much more evolved, with massive cluster formation well underway. The powerful feedback from ongoing star formation has strongly affected the cloud structure in these regions, so observations of the gas do not probe the initial conditions prior to the onset of star formation.

We speculate that $G0.253+0.016$ may be unique in representing the initial conditions of a Galactic molecular cloud on the verge of forming a YMC. As such, its detailed study can reveal important clues about massive cluster formation and help test theoretical models. Current theories suggest that the early evolution of stellar clusters depends crucially on the spatial and kinematic distribution of stars (e.g. Goodwin & Bastian 2006; Allison et al. 2010). However, while the distribution of emergent stellar populations as "hierarchical" or "centrally-condensed" may be straightforward to quantify when analyzing stars, quantifying the small-scale distribution of the gas in a similar way is complicated (see e.g. Lomax et al. 2011). Because gas can not easily be counted in discreet, observationally-defined units, the results of algorithms attempting to quantify gas substructure are notoriously subjective to the values of user-defined inputs (see e.g. Pineda et al. 2009).

Regardless of the exact details of the formation mechanism, the properties of the emergent stellar population must be directly related to the initial global gas properties. Assuming a reasonable star formation efficiency (SFE) (e.g. 30% for gas $\geq 10^4\,{\rm cm}^{-3}$; Alves et al. 2007), $G0.253+0.016$ may form a cluster with stellar mass and density similar to that of other YMCs like the Arches. Whether or not such a cluster remains gravitationally-bound depends on the SFE and environmental conditions (tidal shear, interaction with GMCs etc, e.g. Kruijssen 2011; Elmegreen & Hunter 2010). However, it is clear that $G0.253+0.016$ has enough mass to form an Arches-like cluster without accreting any additional gas or stars from outside the present-day observed boundary.

With only a single candidate YMC precursor it is not possible to determine how representative $G0.253+0.016$ is of all YMC progenitors. It is clearly desirable to search for other proto-YMC molecular clouds, especially within the Galaxy. In the last decade much observational effort has been directed towards searching for, and characterizing the physical properties of molecular clouds which are likely the progenitors of stellar clusters. As a result, a large fraction of the gas in the Galaxy available to form YMCs has been surveyed in dust continuum and dense molecular gas tracers.

Figure 5 summarizes the results from two of these surveys and places $G0.253+0.016$ in the context of Galactic molecular clouds and stellar clusters. Plus symbols show ammonia clumps detected in HOPS (Walsh et al. 2011). The critical density of ammonia is close to the volume density threshold of $\sim 10^4\,{\rm cm}^{-3}$ proposed by Lada et al. (2010) as the threshold required to form stars. As such HOPS is ideal for identifying and characterizing the properties of star forming gas within the Galaxy. Green crosses show IRDCs from the survey of Rathborne et al. (2006). IRDCs are thought to be precursors of high mass stars and clusters. The region of the mass-radius plane covered by the HOPS clouds and IRDCs is similar to that of clouds detected in other surveys, both targeted (e.g. as compiled by Kauffmann & Pillai 2010) and blind, large-area surveys (BGPS – Aguirre et al. (2011); ATLASGAL – Schuller et al. (2009), Tachenberg et al submitted and Beuther et al. priv. comm). The hatched rectangles show the mass-radius range of different stellar clusters (Portegies Zwart et al. 2010) and the black dots show Galactic YMCs. With the exception of a few clouds which may form small YMCs, assuming a reasonable star formation efficiency, most of the observed molecular clouds seem destined to form open clusters. $G0.253+0.016$ is marked with a red star and clearly stands out. It is significantly more massive for its size compared to the other Galactic molecular clouds. It is potentially the only object with an observed gas mass and density which may be able to directly form a cluster with stellar mass and densities in the YMC/globular cluster regime.

The potential uniqueness of $G0.253+0.016$ has profound implications for YMC formation in the Galaxy. We posit three scenarios. If all YMCs form from molecular clouds with similar properties to $G0.253+0.016$, either i) $G0.253+0.016$ is unique in the Galaxy, or, ii) surveys have missed the other similar clouds. Alternatively, iii) if the properties of $G0.253+0.016$ are not representative of other molecular clouds destined to form YMCs, there may be precursors to YMCs in the Galaxy which have already been observed but not identified as YMC precursors.

To distinguish between these scenarios it is important to predict how many proto-YMC molecular clouds are likely to exist at any given time in the Galaxy. One way to estimate this is following the analytical approach of Gieles (2009). Assuming a star formation rate of 1 ${\rm M}_\odot$/yr with 10% of stars forming in clusters and a cluster mass function index of -2, we would expect $\sim$10 clusters of $>10^4\,{\rm M}_\odot$ with ages $<10\,$Myr. This estimate is consistent with the number of YMCs currently known in the Galaxy. If the number of Galactic YMCs is constant, assuming it takes of order a Myr to evolve from precursor to forming cluster we would expect from zero to a few precursors at any given time. An alternative method to estimate the expected number of proto-YMC molecular clouds in the Galaxy is extrapolating the observed embedded cluster mass function (ECMF), which, for embedded clusters up to 10^3 $M_\odot$ within 2 kpc of the Sun, is a power-law with index -2 (Lada & Lada 2003). Assuming this represents the Galactic ECMF (see Gieles 2009), one can scale it to the total volume of the Galactic disk to estimate the number of embedded clusters expected in the Galaxy. Extrapolating this to higher cluster masses, we expect $\sim$ 25 young clusters with masses between 10^4 and 10^5 $M_\odot$. Assuming a cluster lifetime of 10 Myr we predict $\sim$ 2.5 proto-YMCs per Myr in the Galaxy. Both of these approaches suggest there may be other Galactic YMC progenitors. While these estimates are approximate, they predict that only a small number of proto-YMCs should exist in the Galaxy at any given time. However, the uncertainties are sufficiently large that it is not possible to use these estimates to rule out $G0.253+0.016$ as being unique. Therefore, it is currently not possible to distinguish between scenarios i) and ii).

Returning to scenario iii), there are many molecular cloud complexes known with sufficient mass to form YMCs but their present-day gas density is much lower than the expected final YMC stellar density. Examples of these are seen clearly in Figure 5 as clouds with mass $> 10^4\,M_\odot$ and radii $>\sim 8$ pc. Such clouds seem destined to form massive, but unbound, associations. However, it may be possible to form the required YMC stellar densities over time from the convergence of molecular gas flows on large scales and subsequent global gravitational collapse. Indeed, such large-scale gravitational collapse has been directly observed towards a number of massive protoclusters (e.g. W33A (Galván-Madrid et al. 2010), DR21 (Schneider et al. 2010), G10.6 (Keto et al. 1988; Baobab Liu et al. 2010), G8.67 (Longmore et al. 2011)) and is predicted by numerical simulations (Smith et al. 2009; Klessen & Hennebelle 2010). In this scenario, star formation would proceed over several crossing times, leading to a large age spread in cluster members. In this regard, it is interesting to note that an age spread of $\geq$ 10 Myr among cluster members are reported in several YMCs (NGC 3603, NGC 346, 30 Doradus – Beccari et al. 2010; De Marchi et al. 2011a,b). However, there is some debate in the literature over the uncertainty in the age determination of cluster members using this method and whether or not these data are also consistent with age spreads of $\leq$3 Myr (Tobin et al. 2009; Baraffe et al. 2009; Littlefair et al. 2011; Jeffries et al. 2011). Detailed studies of the large-scale gas motions in the youngest and most massive molecular clouds are needed to determine whether the gas/stellar density will increase over time to form YMCs as opposed to more diffuse and gravitationally-unbound OB associations as would be predicted by their current global gas density.

With this scenario in mind, it is interesting to note that large-scale emission from shocked-gas tracers is detected towards $G0.253+0.016$. Combined with gas temperatures of 80 K (Lis et al. 2001, Rathborne et al. in prep), which is much warmer than the dust temperature, this suggests $G0.253+0.016$ may have formed from a cloud-cloud collision or convergence of large scale flows. As the gas has not yet had the chance to heat up the dust, this must have happened recently. If this is the case, before the postulated collision/convergence, the gas properties of $G0.253+0.016$ may have been much more similar to the typical Galactic molecular cloud population and thus may not have stood out as extreme in Figure 5.

Given the location of $G0.253+0.016$ near to the Galactic center, it is tempting to invoke the extreme conditions at the Galactic center (e.g. interstellar radiation field enhanced by 10^3, external pressure P/k$\sim$$10^8$, strong magnetic fields, gamma rays) to justify why it may be unique. In this regard it is interesting to note that $G0.253+0.016$ lies at a projected distance of only 18 pc from the Arches and Quintuplet clusters. While it is not possible to directly link the formation of the Arches with $G0.253+0.016$, it seems plausible that the Arches could have formed at its present distance from the Galactic center. On larger scales $G0.253+0.016$ appears to be part of a $10^6\,M_\odot$ filament of interconnected clumps of which $G0.253+0.016$ is the most massive (Lis et al. 2001). This filament is itself thought to be part of the $3\times10^7\,M_\odot$, 100 pc ring identified by Molinari et al. (2011). The 100 pc ring is orbiting the Galactic center at $\sim$80 kms^{-1} so a single orbit would take $\sim$3.6 Myr. Given the free-fall time for $G0.253+0.016$ is <1 Myr (see Table 2), it seems unlikely $G0.253+0.016$ would survive a whole orbit without additional support – not implausible given the extreme conditions at the Galactic center. If such additional support could be maintained against the rapid turbulent energetic decay, this may explain why the cloud has remained dense and starless.

Alternatively, the fate of the $G0.253+0.016$ may be more intimately linked to the dynamics of the 100 pc ring. Gas is thought to enter the ring at the intersection points of the innermost stable X1 orbits and the X2 orbits. These intersection or "crashing" points coincide with Sgr B2 and Sgr C – the only places in the 100 pc ring with prodigious star formation activity. If the gas comprising $G0.253+0.016$ were to have entered the 100 pc ring at Sgr C it would have joined only a small fraction of an orbit time ago. In around a free-fall time, the whole $10^6\,M_\odot$ filament in which $G0.253+0.016$ is located will have reached the position of Sgr B2. As such, this larger filament could be in the process of forming a $10^6\,M_\odot$, Sgr B2-like complex.

However, while it is tempting to invoke the extreme conditions at the Galactic center to justify why $G0.253+0.016$ may be unique, several of the most massive YMCs in the Galaxy are not located near the Galactic center suggesting the extreme environmental conditions are not a necessary condition to form a YMC.

5. CONCLUSIONS

We make use of existing multi-wavelength data including recently available far-IR continuum (Herschel/Hi-GAL) and mm spectral line (HOPS and MALT90) data and present new, deep, multiple-filter, near-IR (VLT/NACO) observations to study the infrared-dark cloud $G0.253+0.016$. From these data we have derived the global properties of $G0.253+0.016$. It has a high mass ($M_{\rm dust}$ $\sim$ $1.3\times10^5\,M_\odot$), low dust temperature ($\sim$23 K), small radius ($\sim$2.8 pc), high volume density ($7.3\times10^4\,\mathrm{cm}^{-3}$) and high column density ($3.5\times10^{23}\,\mathrm{cm}^{-2}$). It is close to virial equilibrium with almost no signs of active star formation. As such it appears to be a prime candidate for the initial conditions of a molecular cloud destined to form an Arches-like YMC.

Comparing the properties of G0.253 + 0.016 to other Galactic dense molecular clouds shows it to be extreme. We discuss implications of this for the formation of massive protoclusters and posit three scenarios. If all YMCs form from molecular clouds with similar properties to G0.253 + 0.016, either i) G0.253 + 0.016 is unique in the Galaxy, or, ii) surveys have missed the other similar clouds. Currently it is not possible to distinguish between scenarios i) and ii). Nevertheless, clouds with properties like G0.253 + 0.016 must be very rare in the Galaxy making G0.253 + 0.016 extremely important for testing massive cluster formation models. Alternatively, in scenario iii) the properties of G0.253 + 0.016 do not represent those of other molecular clouds destined to form YMCs. We note there are many molecular clouds in the Galaxy with sufficient mass to form YMCs but their present-day gas density is much lower than the expected YMC stellar densities. However, it may be possible to form the required stellar densities over time from the convergence of molecular gas flows on large scales and subsequent global gravitational collapse, as observed towards several lower-mass protoclusters. Detailed studies of the large-scale gas motions in the youngest and most massive molecular clouds are needed to determine whether the gas/stellar density will increase over time to form YMCs as opposed to more diffuse and gravitationally-unbound OB associations as would be predicted by their current global gas density.

In future work we will study the internal structure and kinematics of G0.253 + 0.016 in detail to investigate its recent dynamical history, test the plausibility that it formed from cloud-cloud collisions or converging large-scale flows, and directly test models of massive protocluster formation.

6. ACKNOWLEDGMENTS

We thank the anonymous referee for constructive comments that improved the manuscript. SNL would like to thank Jens Kauffmann, Thushara Pillai, Qizhou Zhang, Henrik Beuther, Peter Schilke and Adam Ginsburg for useful discussions. This research made use of the NASA Astrophysical Data System. The research leading to these results has received funding from the European Community's Seventh Framework Programme (/FP7/2007-2013/) under grant agreement No 229517.

REFERENCES

Aguirre, J. E., Ginsburg, A. G., Dunham, M. K., & et al. 2011, ApJS, 192, 4
Allison, R. J., Goodwin, S. P., Parker, R. J., Portegies Zwart, S. F., & de Grijs, R. 2010, MNRAS, 407, 1098
Alves, J. & Homeier, N. 2003, ApJL, 589, L45
Alves, J., Lombardi, M., & Lada, C. J. 2007, A&A, 462, L17
Ascenso, J., Alves, J., Beletsky, Y., & Lago, M. T. V. T. 2007, A&A, 466, 137
Ashman, K. M. & Zepf, S. E. 2001, AJ, 122, 1888
Bally, J., Aguirre, J., Battersby, C., & et al. 2010, ApJ, 721, 137
Balser, D. S., Rood, R. T., Bania, T. M., & Anderson, L. D. 2011, ApJ, 738, 27
Baobab Liu, H., Ho, P. T. P., Zhang, Q., Keto, E., Wu, J., & Li, H. 2010, ApJ, 722, 262
Baraffe, I., Chabrier, G., & Gallardo, J. 2009, ApJL, 702, L27
Battersby, C., Bally, J., Ginsburg, A., & et al. 2011, ArXiv e-prints
Beccari, G., Spezzi, L., De Marchi, G., & et al. 2010, ApJ, 720, 1108
Benjamin, R. A., Churchwell, E., Babler, B. L., & et al. 2003, PASP, 115, 953
Bernard, J.-P., Paradis, D., Marshall, D. J., & et al. 2010, A&A, 518, L88+
Bertoldi, F. & McKee, C. F. 1992, ApJ, 395, 140
Beuther, H., Schilke, P., Menten, K. M., & et al. 2002, ApJ, 566, 945
Caswell, J. L., Fuller, G. A., Green, J. A., & et al. 2010, MNRAS, 404, 1029
Clark, J. S., Negueruela, I., Crowther, P. A., & Goodwin, S. P. 2005, A&A, 434, 949
Compiègne, M., Verstraete, L., Jones, A., & et al. 2011, A&A, 525, A103+
Danielson, A. L. R., Swinbank, A. M., Smail, I., & et al. 2011, MNRAS, 410, 1687
Davies, B., Bastian, N., Gieles, M., & et al. 2011, MNRAS, 411, 1386
De Marchi, G., Panagia, N., & Sabbi, E. 2011a, ApJ, 740, 10
De Marchi, G., Paresce, F., Panagia, N., & et al. 2011b, ApJ, 739, 27
Di Francesco, J., Johnstone, D., Kirk, H., MacKenzie, T., & Ledwosinska, E. 2008, ApJS, 175, 277
Dunham, M. K., Rosolowsky, E., Evans, II, N. J., & et al. 2010, ApJ, 717, 1157
Elmegreen, B. G. & Hunter, D. A. 2010, ApJ, 712, 604
Figer, D. F., Kim, S. S., Morris, M., & et al. 1999, ApJ, 525, 750
Figer, D. F., MacKenty, J. W., Robberto, M., & et al. 2006, ApJ, 643, 1166
Foster, J. B., Jackson, J. M., Barris, E., & et al. 2011, ArXiv e-prints
Galván-Madrid, R., Zhang, Q., Keto, E., & et al. 2010, ApJ, 725, 17
Gieles, M. 2009, MNRAS, 394, 2113
Goldsmith, P. F., Lis, D. C., Hills, R., & Lasenby, J. 1990, ApJ, 350, 186
Goodwin, S. P. & Bastian, N. 2006, MNRAS, 373, 752
Hildebrand, R. H. 1983, QJRAS, 24, 267
Hill, T., Burton, M. G., Minier, V., & et al. 2005, MNRAS, 363, 405
Holtzman, J. A., Faber, S. M., Shaya, E. J., & et al. 1992, AJ, 103, 691
Jackson, J. M., Foster, J., Brooks, K., Rathborne, J., & Longmore, S. 2011, in American Astronomical Society Meeting Abstracts, Vol. 218, American Astronomical Society Meeting Abstracts 218, 217.02–+
Jackson, J. M., Rathborne, J. M., Shah, R. Y., & et al. 2006, ApJS, 163, 145
Jeffries, R. D., Littlefair, S. P., Naylor, T., & Mayne, N. J. 2011, MNRAS, 1538
Johnson, K. E. & Kobulnicky, H. A. 2003, ApJ, 597, 923
Kauffmann, J., Bertoldi, F., Bourke, T. L., Evans, II, N. J., & Lee, C. W. 2008, A&A, 487, 993
Kauffmann, J. & Pillai, T. 2010, ApJL, 723, L7
Keto, E. R., Ho, P. T. P., & Haschick, A. D. 1988, ApJ, 324, 920
Klessen, R. S. & Hennebelle, P. 2010, A&A, 520, A17+
Kruijssen, J. M. D. 2011, ArXiv e-prints
Lada, C. J. & Lada, E. A. 2003, ARA&A, 41, 57
Lada, C. J., Lombardi, M., & Alves, J. F. 2010, ApJ, 724, 687
Lawrence, A., Warren, S. J., Almaini, O., & et al. 2007, MNRAS, 379, 1599
Lis, D. C. & Menten, K. M. 1998, ApJ, 507, 794
Lis, D. C., Menten, K. M., Serabyn, E., & Zylka, R. 1994, ApJL, 423, L39
Lis, D. C., Serabyn, E., Zylka, R., & Li, Y. 2001, ApJ, 550, 761

TABLE 2
GLOBAL PROPERTIES OF G0.253+0.016. THE COLUMNS SHOW MASS (M), DISTANCE (D), RADIUS (R), DUST TEMPERATURE (T_{dust}), LINEWIDTH (ΔV), VOLUME DENSITY (ρ), COLUMN DENSITY (N_{H_2}), CLOUD-CROSSING TIME (t_{cc}), SOUND-CROSSING TIME (t_{sc}) AND FREE-FALL TIME (t_{ff}).

M ($M_\odot$)	D (kpc)	R (pc)	T_{dust} (K)	ΔV (km/s)	ρ (cm^{-3})	N_{H_2} (cm^{-2})	t_{cc} (Myr)	t_{sc} (Myr)	t_{ff} (Myr)
1.3E5	8.4	2.8	19-27	16	7.3E4	3.5E23	0.17	8	0.74

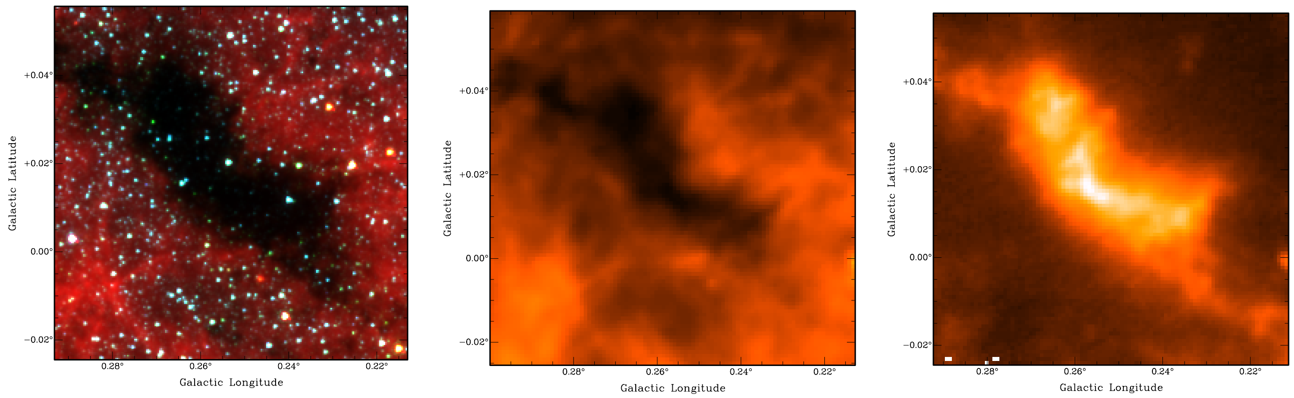

FIG. 1.— Continuum images toward G0.253+0.016. The images are 14 pc on a side for the distance of 8.4 kpc. *Left to right:* GLIMPSE (Benjamin et al. 2003) three color (3.6, 4.5 and 8 μm), Herschel 70 μm (Molinari et al. 2011), SCUBA/JCMT 450 μm (Di Francesco et al. 2008). The cloud G0.253+0.016, is seen as an extinction feature in the mid-IR to far-IR but is a strong emitter in the sub-mm/mm. As such it must be both cold and dense and sit in front of the majority of the diffuse Galactic mid-IR background emission.

Littlefair, S. P., Naylor, T., Mayne, N. J., Saunders, E., & Jeffries, R. D. 2011, MNRAS, 413, L56
Lomax, O., Whitworth, A. P., & Cartwright, A. 2011, MNRAS, 412, 627
Longmore, S. N., Burton, M. G., Barnes, P. J., & et al. 2007, MNRAS, 379, 535
Longmore, S. N., Pillai, T., Keto, E., Zhang, Q., & Qiu, K. 2011, ApJ, 726, 97
Lucas, P. W., Hoare, M. G., Longmore, A., & et al. 2008, MNRAS, 391, 136
MacLaren, I., Richardson, K. M., & Wolfendale, A. W. 1988, ApJ, 333, 821
Maeda, Y., Baganoff, F. K., Feigelson, E. D., Morris, M., Bautz, M. W., Brandt, W. N., Burrows, D. N., Doty, J. P., Garmire, G. P., Pravdo, S. H., Ricker, G. R., & Townsley, L. K. 2002, ApJ, 570, 671
Molinari, S., Bally, J., Noriega-Crespo, A., & et al. 2011, ApJL, 735, L33+
Molinari, S., Swinyard, B., Bally, J., & et al. 2010a, A&A, 518, L100+
—. 2010b, PASP, 122, 314
Najarro, F., Figer, D. F., Hillier, D. J., Geballe, T. R., & Kudritzki, R. P. 2009, ApJ, 691, 1816
Nishiyama, S., Nagata, T., Sato, S., & et al. 2006, ApJ, 647, 1093
Peretto, N. & Fuller, G. A. 2009, A&A, 505, 405
Pillai, T., Wyrowski, F., Carey, S. J., & Menten, K. M. 2006, A&A, 450, 569
Pineda, J. E., Rosolowsky, E. W., & Goodman, A. A. 2009, ApJL, 699, L134
Portegies Zwart, S. F., McMillan, S. L. W., & Gieles, M. 2010, ARA&A, 48, 431
Purcell, C. R., Balasubramanyam, R., Burton, M. G., & et al. 2006, MNRAS, 367, 553
Purcell, C. R., Longmore, S. N., Burton, M. G., & et al. 2009, MNRAS, 394, 323
Rathborne, J. M., Jackson, J. M., & Simon, R. 2006, ApJ, 641, 389
Rathborne, J. M., Johnson, A. M., Jackson, J. M., Shah, R. Y., & Simon, R. 2009, ApJS, 182, 131
Reid, M. J., Menten, K. M., Zheng, X. W., & et al. 2009, ApJ, 700, 137
Santangelo, G., Testi, L., Gregorini, L., & et al. 2009, A&A, 501, 495
Schneider, N., Csengeri, T., Bontemps, S., & et al. 2010, A&A, 520, A49+
Schödel, R., Najarro, F., Muzic, K., & Eckart, A. 2010, A&A, 511, A18+
Schuller, F., Menten, K. M., Contreras, Y., & et al. 2009, A&A, 504, 415
Shields, J. C. & Ferland, G. J. 1994, ApJ, 430, 236
Simon, R., Jackson, J. M., Rathborne, J. M., & Chambers, E. T. 2006a, ApJ, 639, 227
Simon, R., Rathborne, J. M., Shah, R. Y., Jackson, J. M., & Chambers, E. T. 2006b, ApJ, 653, 1325
Smith, R. J., Longmore, S., & Bonnell, I. 2009, MNRAS, 400, 1775
Sridharan, T. K., Beuther, H., Schilke, P., Menten, K. M., & Wyrowski, F. 2002, ApJ, 566, 931
Stead, J. J. & Hoare, M. G. 2009, MNRAS, 400, 731
Swinbank, A. M., Smail, I., Longmore, S., & et al. 2010, Nature, 464, 733
Taylor, M. B. 2005, in Astronomical Society of the Pacific Conference Series, Vol. 347, Astronomical Data Analysis Software and Systems XIV, ed. P. Shopbell, M. Britton, & R. Ebert, 29–+
Tobin, J. J., Hartmann, L., Furesz, G., Mateo, M., & Megeath, S. T. 2009, ApJ, 697, 1103
Walsh, A. J., Breen, S. L., Britton, T., & et al. 2011, MNRAS, 416, 1764
Walsh, A. J., Lo, N., Burton, M. G., & et al. 2008, PASA, 25, 105
Whitmore, B. C. 2000, ArXiv Astrophysics e-prints

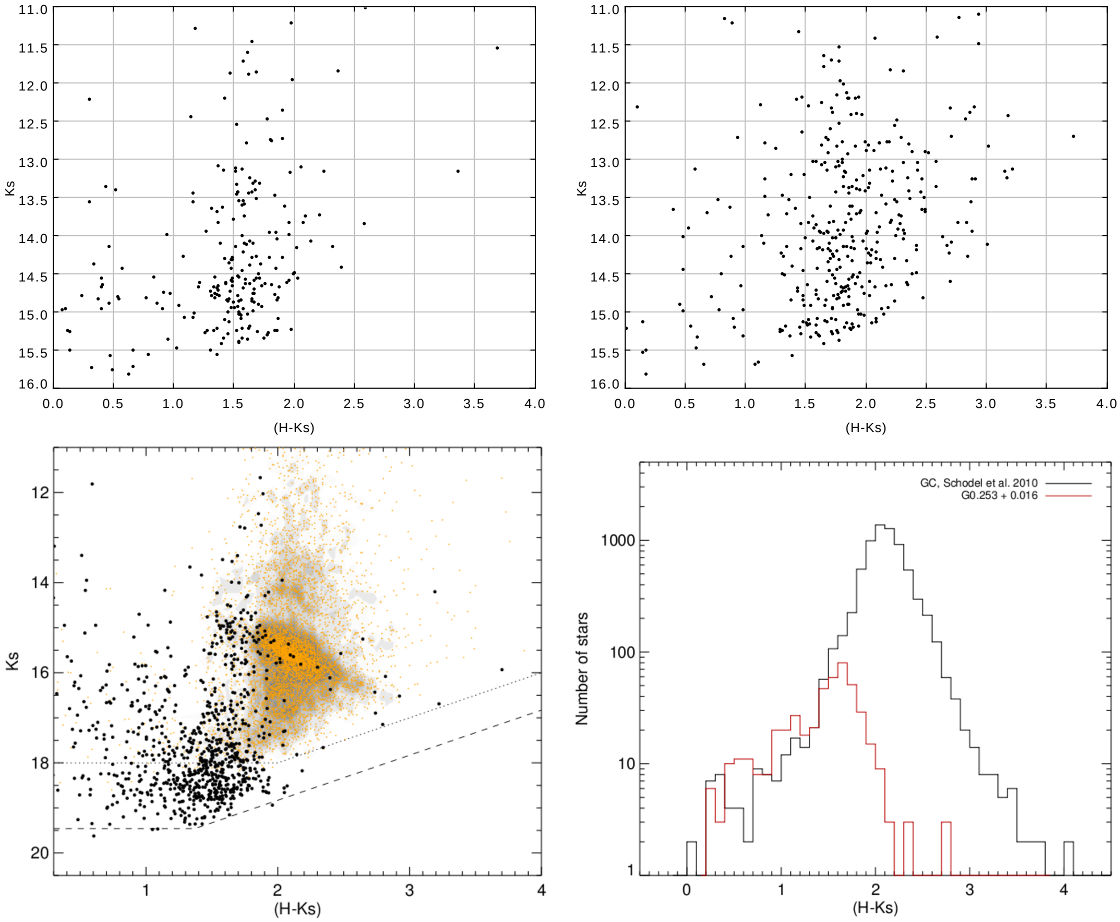

FIG. 2.— [Top panel] K_s *vs.* $(H - K_s)$ color-magnitude diagrams for UKIDSS sources within a circle of radius 45″ centered on G0.253 + 0.016 [left] and an offset position at $l = 0.32°$, $b = -0.02°$ [right]. Although the UKIDSS data are confusion-limited in sensitivity and not as deep as the NACO data (bottom panel) a clear decrease in source counts towards G0.253 + 0.016 is seen at $H - K_s \sim 1.7 \pm 0.2$ mag. [Bottom left panel] K_s *vs.* $(H - K_s)$ color-magnitude diagram. The black dots show sources detected in the VLT/NACO data towards G0.253 + 0.016 (see § 2.2 & 3.1). The yellow dots and grey scale show the VLT/NACO sources and number density, respectively, detected towards the Galactic center from Schödel et al. (2010). Both VLT/NACO observations have the same $1' \times 1'$ field of view but the G0.253 + 0.016 observations are ∼2 mag deeper (as illustrated by the dotted and dashed lines showing the approximate 5σ sensitivity limits of the Schödel et al. (2010) and G0.253 + 0.016 datasets, respectively). In the Schödel et al. (2010) data, the red giant branch bump feature continues to $(H - K_s) \sim 2.4$ mag and is still visible at 2.6 mag, where it becomes strongly effected by completeness limits. Despite being ∼2 mag deeper and looking along similar lines of sight (and hence similar foreground extinction and expected stellar populations), the red giant branch bump feature is sharply truncated in the G0.253 + 0.016 observations. [Bottom right panel] Histogram of the $(H - K_s)$ colors for the Schödel et al. (2010) catalog [black], and for the NACO sources in G0.253 + 0.016 brighter than the Schödel et al. (2010) detection limit [red]. Both distributions are similar for $(H - K_s) \leq 1.7$ but the number of G0.253 + 0.016 sources shows a sharp cutoff at redder colors, despite the observations being ∼2 mag deeper. This is clear evidence that we have detected the extinction from G0.253 + 0.016, and that this is a single entity as opposed to multiple clouds along the line of sight. The distance determined from these data is consistent with G0.253 + 0.016 being in close proximity to the Galactic center (§ 3.1).

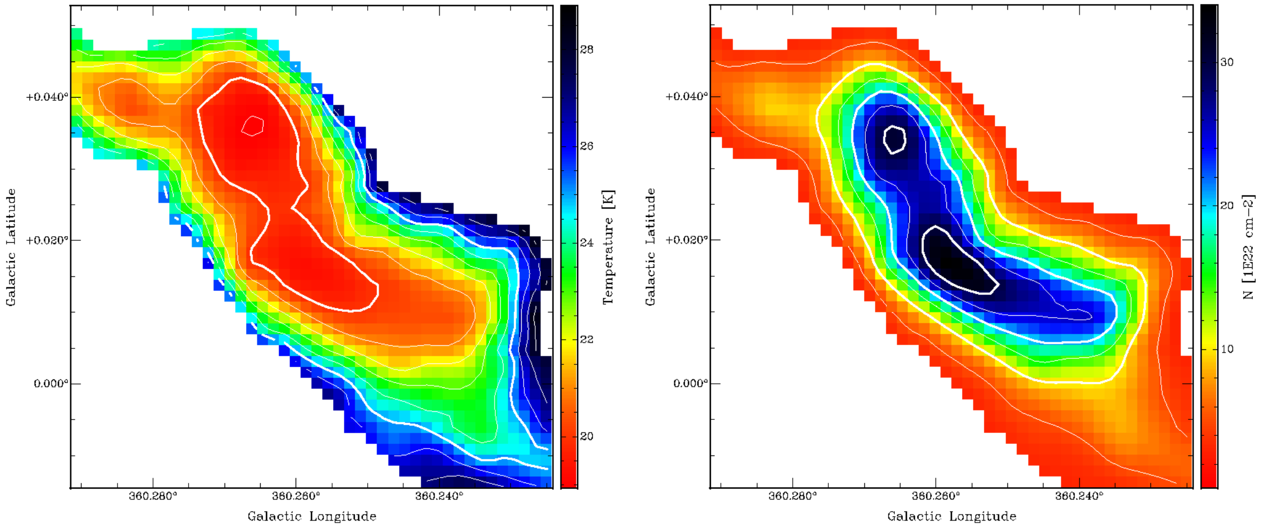

Fig. 3.— Dust temperature [left] and column density [right] maps of G0.253 + 0.016 derived from the Hi-GAL data. The images are 12 pc on a side for the distance of 8.4 kpc. The temperature contours are 19, 20, ..., 28 K and the column density contours are 5, 10, ..., 35 $\times 10^{22}$ cm^{-2}. The color scale shows all pixels above the threshold column density of 3×10^{22} cm^{-2} used to define the boundary of G0.253 + 0.016 (see § 3.2). The dust temperature overall is low, increasing smoothly from $\sim$19 K at the center to $\sim$27 K at the edge. There are no obvious small pockets of heated dust from any embedded sources. The derived external temperature of G0.253 + 0.016 is significantly warmer ($\gtrsim$35 K). The column density and dust temperature are anticorrelated as expected for an externally-heated, dense clump. The derived peak column density is $\sim3.3\times10^{23}$ cm^{-2} which decreases smoothly towards the edge. The average column density in the region above the threshold cutoff is $\sim1\times10^{23}$ cm^{-2}. Based on the column density maps we derive G0.253 + 0.016's effective radius and mass to be 2.8 pc and 1.3×10^{5} M$_{\odot}$, respectively.

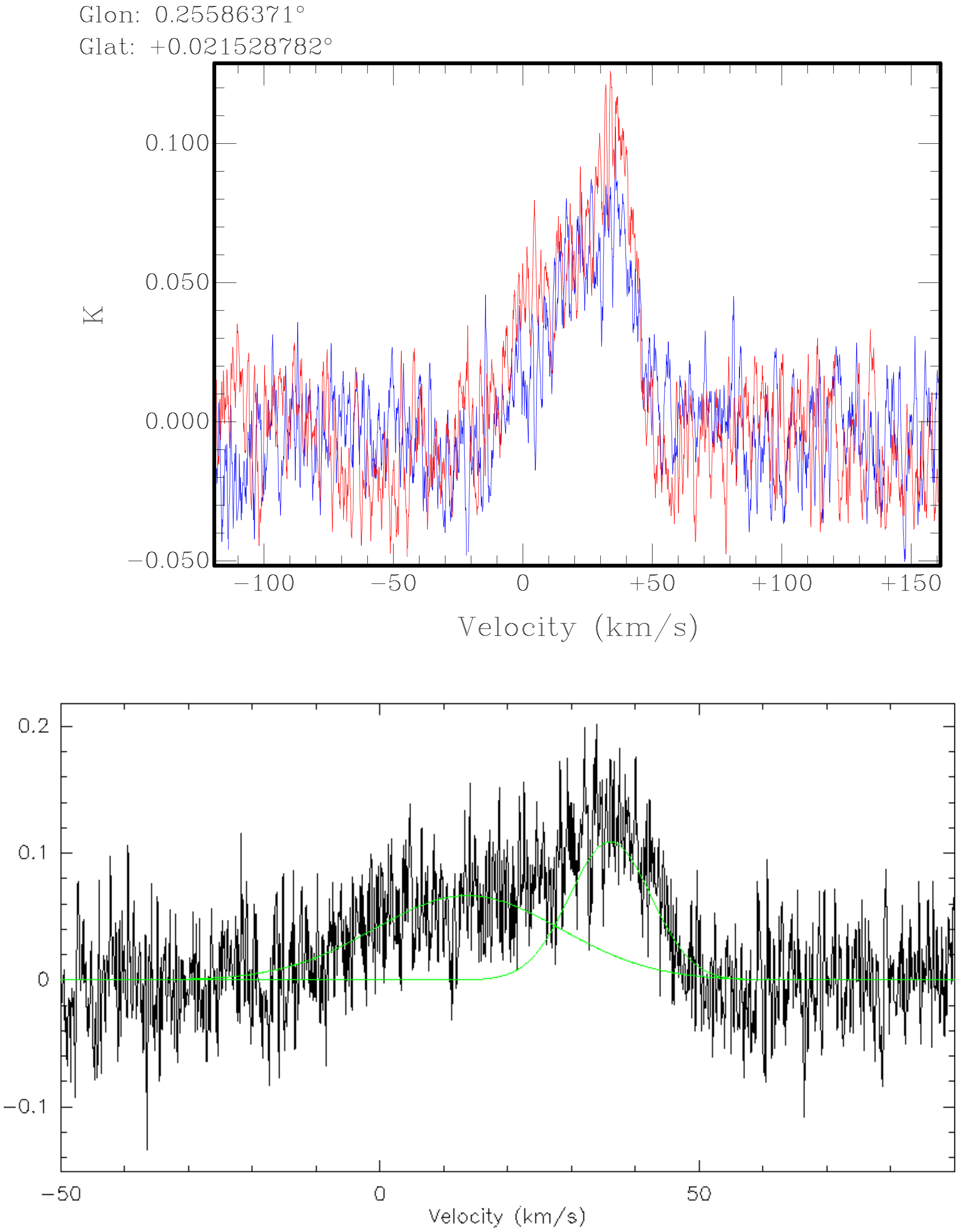

FIG. 4.— [Top] Hanning-smoothed $H^{13}CO^+$(1-0) [blue] and $HN^{13}C$(1-0) [red] spatially-averaged spectra across G0.253 + 0.016 from the MALT90 survey. Emission from both these transitions is expected to be optically-thin so should reliably trace the underlying gas kinematics. The line profiles for both transitions are similar, with two components: a brighter one at $V_{\rm lsr} = 35\,{\rm km s^{-1}}$ from G0.253 + 0.016 and a weaker one at $V_{\rm lsr} = 0\,{\rm km s^{-1}}$ from an unrelated cloud along the line of sight. [Bottom] The black line shows the same $HN^{13}C$(1-0) line profile as above, but without any Hanning smoothing. The green line shows the results of a two-component Gaussian fit to this profile, from which a line FWHM of $15.1 \pm 1.0\,{\rm km s^{-1}}$ is derived for the gas associated with G0.253 + 0.016.

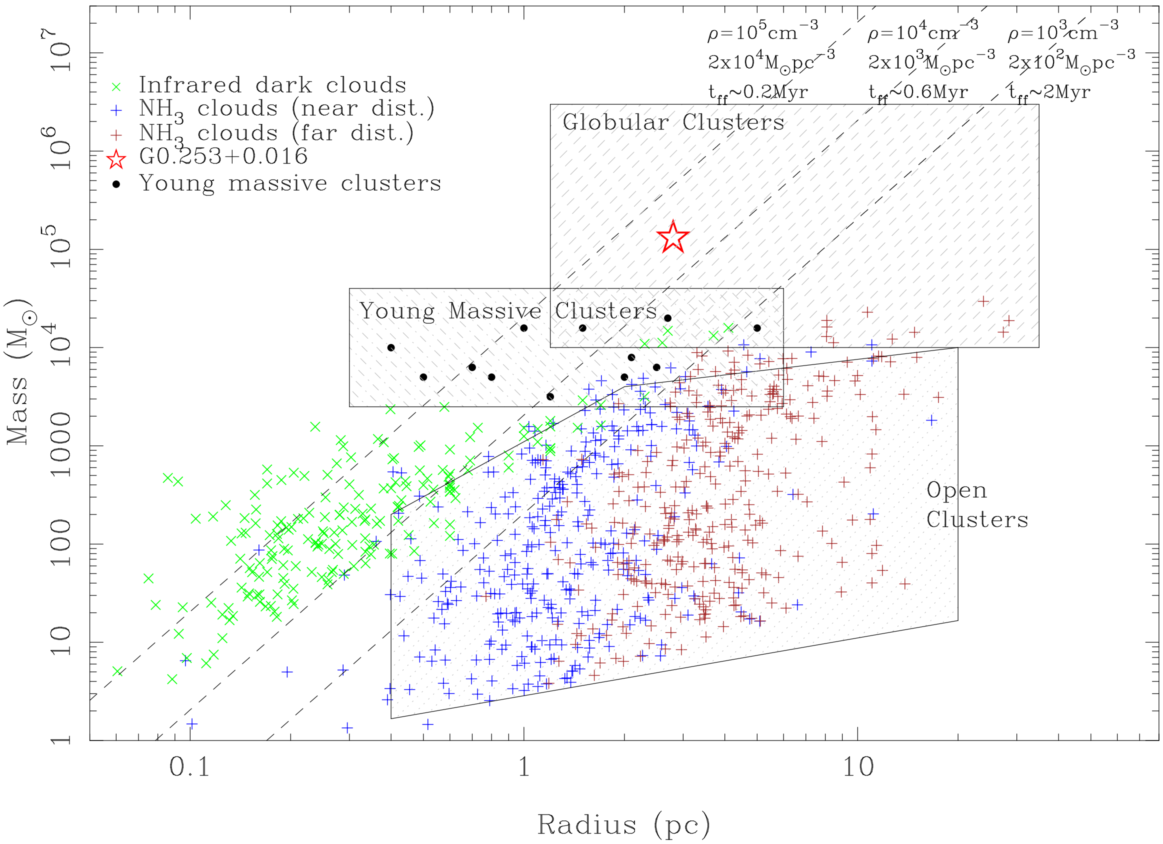

Fig. 5.— Radius versus mass for Galactic dense, cluster-forming molecular clouds. Plus symbols show ammonia clouds detected in HOPS (Walsh et al. 2011) (blue/brown denote an assumed near/far kinematic distance, respectively). Green crosses show infrared dark clouds (IRDCs) from the survey of Rathborne et al. (2006). The hatched rectangles show the mass-radius range of different stellar clusters (Portegies Zwart et al. 2010). The black dots show Galactic young massive clusters. With the exception of a few clouds which may form small YMCs, assuming a reasonable star formation efficiency, most of the observed molecular clouds seem destined to form open clusters. G0.253 + 0.016 is marked with a red star and clearly stands out as unique. It has a mass and radius that would be expected of a molecular cloud progenitor of a large YMC or a globular cluster. The dashed lines show constant density and free-fall time.